ARTICLE OPEN ACCESS

The Role of Structural Flexibility in Hydrocarbon-Stapled Peptides Designed to Block Viral Infection via Human ACE2 Mimicry

Sicheng Jiang[1] | Yu Tian[1] | Vlad Nicolaescu[2] | Aslan Mansurov[1] | Glenn Randall[2] | Matthew V. Tirrell[1,2] | James L. LaBelle[3] (ID)

[1]Pritzker School of Molecular Engineering, The University of Chicago, Chicago, Illinois, USA | [2]Argonne National Laboratory, Lemont, Illinois, USA | [3]Department of Pediatrics, Section of Hematology/Oncology, The University of Chicago, Chicago, Illinois, USA

Correspondence: Matthew V. Tirrell (mtirrell@uchicago.edu) | James L. LaBelle (jlabelle@bsd.uchicago.edu)

ABSTRACT

The COVID-19 pandemic drove a uniquely fervent pursuit to explore the potential of peptide, antibody, protein, and small-molecule-based antiviral agents against severe acute respiratory syndrome-coronavirus 2 (SARS-CoV-2). The interaction between the SARS-CoV2 spike protein with the angiotensin-converting enzyme 2 (ACE2) receptor that mediates viral cell entry was a particularly interesting target given its well-described protein–protein interaction (PPI). This PPI is mediated by an α-helical portion of ACE2 binding to the receptor binding domain (RBD) of the spike protein and thought to be susceptible to blockade through molecular mimicry. Small numbers of hydrocarbon-stapled synthetic peptides designed to disrupt or block this interaction were tested individually and were found to have variable efficacy despite having related or overlapping sequences and similarly increased α-helicity. Reasons for these differences are unclear and reported preclinical successes have been limited. This study sought to better understand reasons for these differences through evaluation of a comprehensive collection of hydrocarbon-stapled peptides, designed based on four distinct principles: stapling position, number of staples, amino acid sequence, and primary sequence length. Surprisingly, we observed that the helicity and amino acid sequence iterations of hydrocarbon-stapled peptides did not correlate with their bioactivity. Our results highlight the importance of iterative and combinatorial testing of these compounds to determine a configuration that best mimics natural binding and allows for chain flexibility while sacrificing structural helicity.

1 | Introduction

Severe acute respiratory syndrome coronavirus 2 (SARS-CoV-2) was responsible for the global outbreak of coronavirus disease 2019 (COVID-19), which caused a profound worldwide healthcare crises [1]. COVID infection presents with a broad range of symptoms, including fever, cough, and respiratory distress, often necessitating hospitalization for oxygen support and assisted ventilation in severe cases. The unprecedented surge in healthcare demand during the peak of the pandemic exerted immense strain on healthcare infrastructures, prompting a rapid and intensive research effort aimed at developing novel and targeted antiviral therapeutics specifically tailored to combat this viral pathogen [2].

The viral infection by SARS-CoV-2 is initiated through a critical protein–protein interaction (PPI) involving the receptor binding domain (RBD) of the spike glycoprotein (S-protein) and

the angiotensin-converting enzyme 2 (ACE2) receptor, which is prominently expressed on epithelial cells of many tissues including the heart, blood vessels, kidneys, liver, gastrointestinal tract, and lungs [3]. Cryo-electron microscopy (cryo-EM) rapidly elucidated the crystal structure of this PPI (Figure 1a). This structure provided evidence that the interaction between the two proteins is predominantly facilitated by the ACE2 helix α1. The ACE2 helix α1 encompasses several crucial amino acids that engage in side chain interactions, with the viral S-protein contributing to the molecular SARS-CoV-2 cellular recognition process (Figure 1b) [4].

Following the determination of the S-protein:ACE2 PPI, there were a number of reports which utilized stapling of peptides made in the likeness of helix α1 in an effort to block binding of SARS-CoV-2 to target cells [6–9]. Despite diverse design strategies employed by different groups in testing small numbers of peptides, including stapling of different primary sequence lengths (22-mer [7] to 35-mer [10]), utilization of different staple lengths (i, $i+4$ or i, $i+7$ [8]), and so forth, there has been mixed results in terms of downstream efficacy against either pseudo virus or authentic SARS-CoV-2, with the best-performing peptide candidates displaying micromolar IC_{50} values [11].

The primary objective of this study was to elucidate the underlying challenges associated with targeting this specific PPI using hydrocarbon-stapled peptides when tested against one another. In this context, we present a comprehensive and systematic compilation of stapled peptides designed and synthesized based on various design parameters. Additionally, we employ orthogonal characterization techniques to evaluate their secondary structures and therapeutic effectiveness. Through our analysis, we determined key design principles that play pivotal roles in determining efficacy of this class of molecules against the SARS-CoV-2 target. We believe our work sheds light on determining why previous attempts to target this PPI with stapled peptides have proven challenging and may help illuminate future strategies to drug similar PPIs with stapled peptides.

2 | Materials and Methods

All experiments mentioned in this article were performed in accordance with the standard safety guidelines of The University of Chicago Environmental Health & Safety.

2.1 | Peptide Synthesis Reagents

All chemicals utilized in this study were used as received are as follows: Amino acids, N,N-diisopropylethylamine (DIPEA), the activating reagent (1-[bis(dimethylamino)methylene]-1H-1,2,3-triazolo[4,5-b]pyridinium 3-oxide hexafluorophosphate [HATU]), Grubbs catalyst, acetic anhydride (Ac$_2$O), piperidine, triisopropylsilane (TIS), trifluoroacetic acid (TFA), unnatural amino acid (S)-N-Fmoc-2-(4′-pentenyl) alanine (S5), 1,2-dichloroethane (DCE), fluorescein isothiocyanate isomer I (FITC), and rink amide resin LL (100–200 mesh, 0.26 mmol/g loading) were purchased from Millipore Sigma. N,N-dimethylformamide (DMF), N-methyl-2-pyrrolidone (NMP), and dichloromethane (DCM) were purchased from Gyros Protein Technologies. Diethyl ether, acetonitrile (ACN) was purchased from Thermo Fisher Scientific.

2.2 | Peptide Synthesis and Purification

Hydrocarbon-stapled peptides were synthesized using standard Fmoc solid-phase peptide synthesis (SPPS) [12–16]. In brief, peptides were prepared at a 200 µmol scale on rink amide resin using an automated synthesizer (Prelude X, Gyros Protein Technologies). The automatic synthesizer proceeded as follows unless otherwise specified: The resins were swelled in DMF for 30 min, then were deprotected for 20 min with 20% piperidine in NMP. The coupling reaction was conducted for 60 min with 10 eq. of the appropriate amino acid dissolved in NMP at 0.3 M, 9.5 eq. HATU dissolved in NMP at 0.285 M, and 20 eq. DIPEA dissolved in NMP at 0.6 M. After each coupling step, a capping solution (4:1:0.1 NMP/Ac$_2$O/
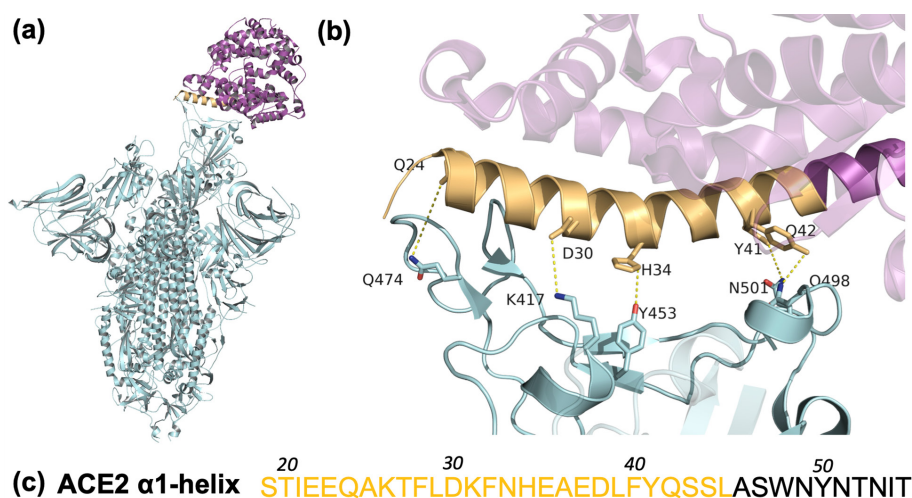
FIGURE 1 | Structural interactions between SARS-CoV-2 spike glycoprotein and human ACE2 receptor. (a) Crystal structure of the SARS-CoV-2 spike glycoprotein (S-protein) (cyan) with the human ACE2 receptor (purple) bound (PDB: 7A94 [5]). The ACE2 helix α1 is highlighted in orange. (b) PPI interface of interest between critical residues of ACE2 helix α1 and the RBD of the SARS-CoV-2 spike glycoprotein (S-protein) with main interacting amino acid side chains depicted. (c) The human ACE2 helix α1 native amino acid sequence.

DIPEA) was applied for 10 min to cap any unreacted chains. Five washes were performed in between steps with alternating DMF/DCM.

Hydrocarbon stapling was achieved by replacing the corresponding residues with α,α-disubstituted non-natural amino acid S5, followed by four rounds of ring closing metathesis reaction catalyzed by 8 mL of 1st generation Grubbs catalyst (4 mg/mL in DCE) for 3 h. Double-stapled peptides were synthesized in a similar fashion as previously reported [17]. Following the last deprotection step, peptide acetylation was achieved by incubation with the capping solution for 20 min. Portions of Fmoc-protected resin were deprotected, coupled with beta-alanine, then FITC-functionalized before cleavage.

Peptides were cleaved in a cleavage cocktail (95:2.5:2.5 TFA:TIS:water) for 2 h. The final peptide was precipitated by adding the cleaved peptides to ice-cold diethyl ether. The mixture was centrifuged, and the supernatant discarded. The resulting peptide was then resuspended in a 1:1 mixture of ACN and water for reverse phase HPLC (RP-HPLC) purification using a Shimadzu system with a waters column (C18, Xbridge BEH OBD Prep column, 19 mm × 150 mm, 5 μm particle size and 130 Å pore size). All peptides used in this study were >95%. LCMS traces for all peptides are shown in Figures S1 and S2. Concentrations of purified peptides were determined through amino acid analysis (Proteomics Core Facility, University of California Davis, Davis, CA).

2.3 | Circular Dichroism

Secondary structure was analyzed using a circular dichroism (CD) spectrometer (J-815, JASCO Corporation) similarly as previously described [14, 18]. Briefly, sample solutions were prepared at 25 μM concentration in 10 mM phosphate buffer (pH = 7.4) and transferred into an absorption cuvette with 1 mm path length (110-QS, Hellma, Inc.). Pure buffer solutions were used for the background correction. Unless otherwise specified, for full wavelength scans, sample spectra were recorded from 185 to 255 nm at desired temperatures, with a scanning rate of 50 nm/min and averaged over three wavelength scans. Data points for the wavelength-dependent CD spectra were recorded at every 0.05 nm with a 1 nm bandwidth and a 4-s response time for each data point. To measure any potential denaturation and hysteresis, full wavelength scans were performed both increasing and decreasing temperature between 5°C and 95°C at 10°C intervals. The heating/cooling rate was set to 4°C/min, and 1 min was allowed after reaching each temperature point for sample equilibration. The CD data were converted to mean residue ellipticity using the formula [19]:

$$\theta\left(\deg \cdot cm^2 \cdot dmol^{-1}\right) = \frac{\theta(\text{millidegree})}{L(\text{mm}) \cdot c(M) \cdot N}$$

in which, θ is the measured ellipticity in millidegree, L is the pathway length of CD cuvette in millimeter, c is the peptide solution molar concentration in mol/L, N is the number of amino acid residues. The values of θ at 222 nm were used to monitor temperature-dependent behavior and converted to a percent alpha helicity using formula [20]:

$$\%\text{Helicity} = \frac{\theta_{222}}{-400 \cdot \left[1 - \left(\frac{2.5}{\text{number of AAs}}\right)\right] + T(°C)}$$

2.4 | SARS-CoV-2 Spike RBD Production and Purification

Production of the spike protein RBD (Spike319-541; GenBank: MN908947.3) was carried out as previously described [21]. Briefly, expression plasmids on the pCAGGS backbone containing mammalian codon-optimized sequences for this gene were obtained from Florian Krammer's laboratory (Icahn School of Medicine at Mount Sinai, New York, NY). Suspension-adapted HEK-293F cells were maintained in serum-free FreeStyle 293 Expression Medium (Gibco). On the day of transfection, cells were inoculated at a concentration of 1×10^6 cells/mL. Plasmid DNA (1 mg/mL) was mixed with linear 25 kDa polyethyleneimine (2 mg/mL; Polysciences) and co-transfected in OptiPRO SFM Medium (4% final concentration; Gibco). Flasks were cultured in an orbital shaking incubator (135 rpm, 37°C, 5% CO_2) for 7 days. Culture medium was then collected by centrifugation, filtered, and loaded into a HisTrap HP 5 mL column (GE Healthcare) using an ÄKTA Pure 25 (GE Healthcare). After washing the column with wash buffer (20 mM NaH_2PO_4 and 0.5 M NaCl, pH = 8.0), the protein was eluted using a gradient of 500 mM imidazole in wash buffer. The protein was further purified by size-exclusion chromatography using a HiLoad Superdex 200PG column (GE Healthcare) with PBS as an eluent. Dimers of RBD were reduced by the addition of dithiothreitol (1 mM), which was subsequently dialyzed against PBS. All purification steps were carried out at 4°C. The expressed proteins were verified to be >90% pure through SDS-PAGE. Protein concentration was determined by absorbance at 280 nm using a NanoDrop spectrophotometer (Thermo Scientific). Proteins were stored at a concentration of 0.9 mg/mL at −80°C until use.

2.5 | Fluorescence Polarization Assay

Binding between recombinant spike protein and stapled peptides was measured using fluorescence polarization (FPA) similar to previously described [15, 16]. A protein dilution buffer was prepared using the following recipe: 20 mM Tris buffer (pH = 8.0), 150 mM NaCl, 1 mM $MgCl_2$, 0.5 mM tris(2-carboxyethyl)phosphine (TCEP), 0.01% Tween 20 [18]. To prepare the dilution series, the spike RBD protein stock solution was serially diluted six times by 3-fold from 9 μM using the protein dilution buffer. FITC-labeled peptides were first dissolved in DMSO as 10 mM stock solutions, and then diluted in the protein dilution buffer to a final concentration of 25 nM. Peptides were mixed with protein solutions at a 1:9 ratio on black opaque 384-well microplates (Corning) and incubated for 30 min before measurements using a Synergy Neo HST plate reader. The data were fitted to a one-site-specific binding model in Prism to calculate binding constants.

2.6 | Authentic SARS-CoV-2 Inhibition Assay

The viral inhibitory efficacy of all peptides was evaluated with live SARS-CoV-2 virus based on a previously reported method [21]. Five hundred plaque forming units of the SARS-CoV-2 virus (nCoV/Washington/1/2020, kindly provided by N. Thornburg, CDC via the World Reference Center for Emerging Viruses and Arboviruses, Galveston, TX) were incubated with 4×10-fold serial dilutions of all peptides or controls for 1 h in DMEM without fetal bovine serum. Viruses were then loaded onto ACE2-A549 cells (kindly provided by B. R. tenOever, NYU Grossman School of Medicine, New York, NY and validated as previously reported [22]) and incubated for 72 h at low serum conditions (2%) in 96-well clear flat bottom plates (Corning) at a density of 20,000 cells per well. Postinfected cells were washed with PBS, fixed with 10% formalin, and stained with crystal violet to detect remaining live cells. Absorbance of stained cells was quantified at 595 nm using a Tecan Infinite 200Pro plate reader. Absorbance values were then normalized to no treatment controls (0% inhibition) and mock-infected controls (100% inhibition).

3 | Results

3.1 | Peptide Design

Previous reports testing small numbers of hydrocarbon-stapled peptides have explored a multitude of stapling strategies based on the linear sequence of ACE2 α1 helix [7–9]. Existing literature using stapled peptides made in the likeness of the ACE2 α1 helix have shown micromolar affinities and antiviral effectiveness only at considerably high doses, if at all [7–9]. Based upon these results we aimed to identify peptide design parameter(s) that may have limited the efficacy of stapled ACE2 α1 helix peptides in previous reports. To do this, we synthesized an extensive peptide library based upon multiple stapled peptide design principles, including staple position, staple number, and amino acid sequence modifications [12, 23]. The resulting panel of stapled alpha helices (SAH) of the ACE2 α1 helix (SAH-ACE) is summarized in Table 1.

SAHs were designed with one or two i, $i + 4$ hydrocarbon staples. We pursued two primary lengths of peptides based on coverage of the entire ACE2 α1 helix. Native, unstapled, peptides (ACE2[21–43] and ACE2[19–45]) were used as peptide controls to compare effects of stapling on efficacy. The first group of stapled peptides reflected an i, $i + 4$ staple "walk" down the length of the ACE2 α1 helix (sSAH-ACE2-1 to 6) while avoiding substitution of interacting residues responsible for the S-protein:ACE2 PPI interface. These SAHs were designed to explore the effect of stapling position while minimizing undesired steric hindrance to peptide-protein complexation (Figures S3 and S4). A second group of SAHs using the same primary amino acid sequence was designed with two i, $i + 4$ staples (dSAH-ACE2-7 to 10) to determine the effect of enhanced α-helical rigidity on affecting this PPI (Figures S3 and S4). To further test, if distance between the two staples affects their efficacy, another group of dSAHs were iterated by expanding the 23 amino acid base sequence by two residues on both the C- and N-terminus. Here, we aimed to compare the efficacy of SAHs with evenly spaced (dSAH-ACE2-11 to 15) or SAHs with maximally distanced staples (dSAH-ACE2-17 to 21). Lastly, we tested base amino acid sequence alternatives to functionally test published *in silico* screen results suggesting

TABLE 1 | Single and double-stapled SAH-ACE2 peptides tested in this study.

Name	Sequence	Net Charge at pH=7	Name	Sequence	Net Charge at pH=7
ACE2(21–43)	IEEQAKTFLDKFNHEAEDLFYQS	−4	ACE2(19–45)	STIEEQAKTFLDKFNHEAEDLFYQSSL	−4
sSAH-ACE2-1	XEEQXKTFLDKFNHEAEDLFYQS	−4	dSAH-ACE2-11	STXEEQXKTFLDKXNHEXEDLFYQSSL	−4
sSAH-ACE2-2	IXEQAXTFLDKFNHEAEDLFYQS	−4	dSAH-ACE2-12	STXEEQXKTNLDKXNHEXEDLFYQSSL	−4
sSAH-ACE2-3	IEEQAKTXLDKXNHEAEDLFYQS	−4	dSAH-ACE2-13	STXEEQXKLFLDKXNHEXEDLFYQSSL	−4
sSAH-ACE2-4	IEEQAKTFXDKFXHEAEDLFYQS	−4	dSAH-ACE2-14	STXEEQXKTFLEKXNHEXEDLFYQSSL	−4
sSAH-ACE2-5	IEEQAKTFLDKXNHEXEDLFYQS	−4	dSAH-ACE2-15	STXEEQXKTFLDWXNHEXEDLFYQSSL	−5
sSAH-ACE2-6	IEEQAKTFLDKFNHEXEDLXYQS	−4	sSAH-ACE2-16	STIXEQAXTFLDKFNHEAEDLFYQSSL	−4
dSAH-ACE2-7	XEEQXKTFLDKXNHEXEDLFYQS	−4	dSAH-ACE2-17	STIXEQAXTFLDKFNHEAEDLXYQSXL	−4
dSAH-ACE2-8	XEEQXKTFLDKFNHEXEDLXYQS	−4	dSAH-ACE2-18	STIXEQAXTNLDKFNHEAEDLXYQSXL	−4
dSAH-ACE2-9	IEEQAKTFXDKFXHEXEDLXYQS	−4	dSAH-ACE2-19	STIXEQAXLFLDKFNHEAEDLXYQSXL	−4
dSAH-ACE2-10	IEEQAKTXLDKXNHEXEDLXYQS	−4	dSAH-ACE2-20	STIXEQAXTFLEKFNHEAEDLXYQSXL	−4
			dSAH-ACE2-21	STIXEQAXTFLDWFNHEAEDLXYQSXL	−5

Note: Two native human ACE2 sequences of different amino acid stretches encompassing a 23-mer and 27-mer, ACE2 (21–43; left column) and ACE 2 (19–45; right column) respectively, were used as biologic templates for SAH synthesis. Residues critical for the interaction between the SARS-CoV-2 S-protein and the ACE2 helix α1 are marked by red, point mutations by green, and non-natural amino acids at stapling positions with blue letters. X represents (S)-N-Fmoc-2-(4′-pentenyl) alanine or S5. Single-stapled peptides have names beginning with sSAH, whereas double-stapled peptides begin with dSAH.

that certain point mutations, namely, F28N, T27L, D30E, and K31W, would increase affinity to the natural PPI [24, 25].
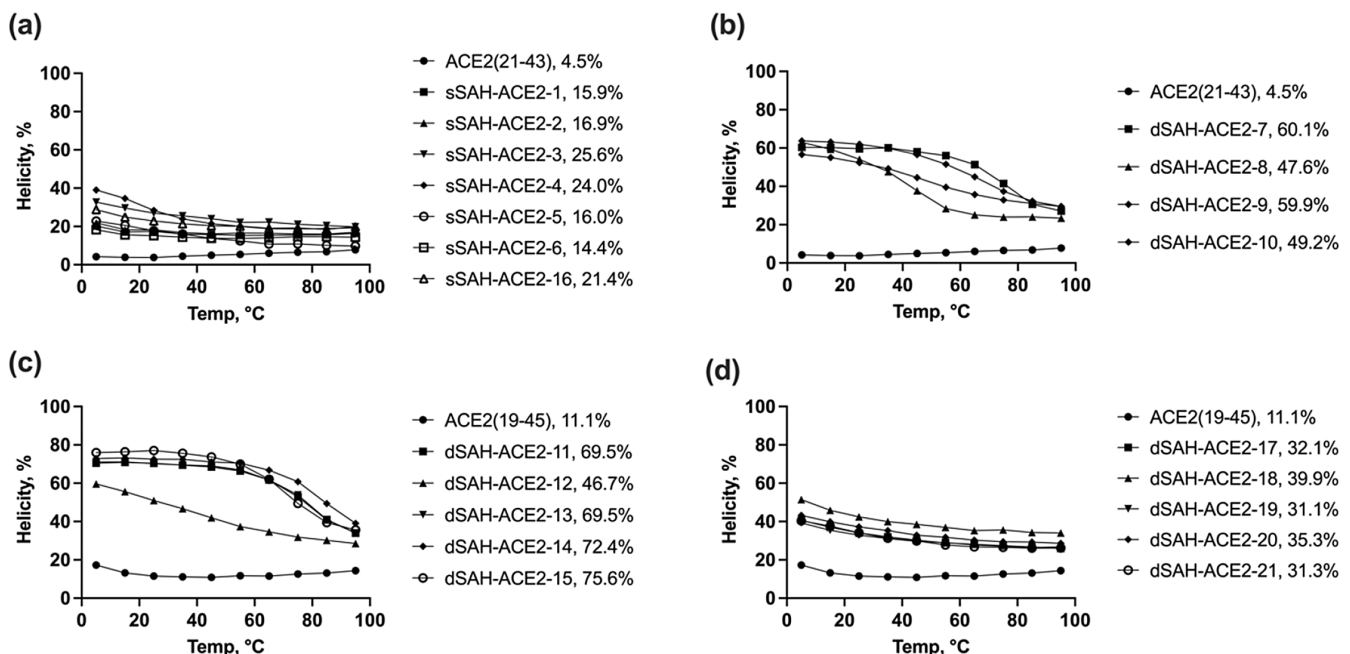
3.2 | Secondary Structure and Thermal Stability in Solution

We next sought to probe the secondary structure and thermal stability of these stapled peptides in an effort to determine how staple position, staple number, and amino acid substitutions affected the α-helical nature of the SAH-ACE2 in the setting of different temperatures. Changes in thermal stability could affect ligand affinity at biologically relevant in vivo temperatures. In addition, while singly stapled peptides are monomeric at normal concentrations used to determine helicity in standard CD analyses [26, 27], it is possible that they have conformational flexibility or even aggregate over broad temperature ranges [17, 28]. Thereby, CD spectra were obtained to measure the percent helicity of unbound peptides in solution at a broad temperature range, including physiologically relevant temperatures. Changes in temperature allowed for using thermal α-helical stability as a proxy for chain flexibility. In this study, control peptides ACE2(21–43) and ACE2(19–45), lacking any stapling modifications, consistently existed as a random coil in solution and with low α-helicity at all temperatures tested, 4.5% and 11.1%, respectively (Figure 2). Short helical peptides typically do not display a pronounced α-helical structure in solution due to the entropic cost of maintaining a restricted conformation outweighing the enthalpic benefit gained from hydrogen bonding within the peptide backbone [29]. The introduction of a single hydrocarbon staple into the ACE2(21–43) sequence resulted in significant enhancements of α-helicity, irrespective of the staple's positional variance. Notably, peptides with central-region stapling

(sSAH-ACE2-3 and sSAH-ACE2-4) manifested the highest increase in α-helicity (25.6% and 24%, respectively), particularly at and below physiological temperatures (37°C), as compared to those with staples positioned closer to the N- or C-terminal ends (Figure 2a). These data, and that of others supports that the ACE2 α1-helix alone is unstructured in solution and is best locked into an α-helical secondary structure when stapled in the middle of the sequence allowing for bidirectional propagation of α-helicity [7–9]. Because of this, we postulated that additional staples would induce greater and more stable α-helicity. Indeed, incorporation of two staples resulted in a significant enhancement of α-helicity across a broad temperature range compared with single-stapled peptides (Figure 2b). However, when the two staples were positioned further apart, it appeared to induce relaxation and increased chain flexibility, consequently resulting in a decrease in helicity and thermal resistance (Figure 2c,d). Thus, staple position and number of staples independently affect α-helicity and structural stability of SAH-ACE2 peptides across a broad range of temperatures. Full CD spectra of each peptide are shown in Figure S5.

3.3 | SAH-ACE2 Affinity for SARS-CoV-2 Spike RBD Protein

We next compared target binding affinity of the SAH-ACE2 panel to target recombinant SARS-CoV-2 spike protein RBD (Spike 319–541) using FPA. While unstapled peptides showed no binding, all SAH-ACE2 peptides displayed micromolar (K_d) binding affinities to RBD, similar to previously reported affinities of similar stapled peptide constructs [7–9]. However, we found all sSAHs failed to reach saturation of binding through the highest concentration of RBD protein used (9 μM) while dSAHs showed

FIGURE 2 | Secondary structure and thermal stability analysis of all ACE2-SAHs by circular dichroism (CD). Percent α-helicities calculated during heating based on the MRE values at 222 nm are plotted as a function of temperature with exact values at 35°C listed in the legends. Heating cycles ranging from 5°C to 95°C is shown. Peptides are plotted on separate panels based on number and position of staples for clarity. (a) single-stapled peptides, (b) double-stapled 23-mers, (c) double-stapled 27-mers with one staple located across the H34 position, (d) double-stapled 27-mers with both staples positioned away from H34.
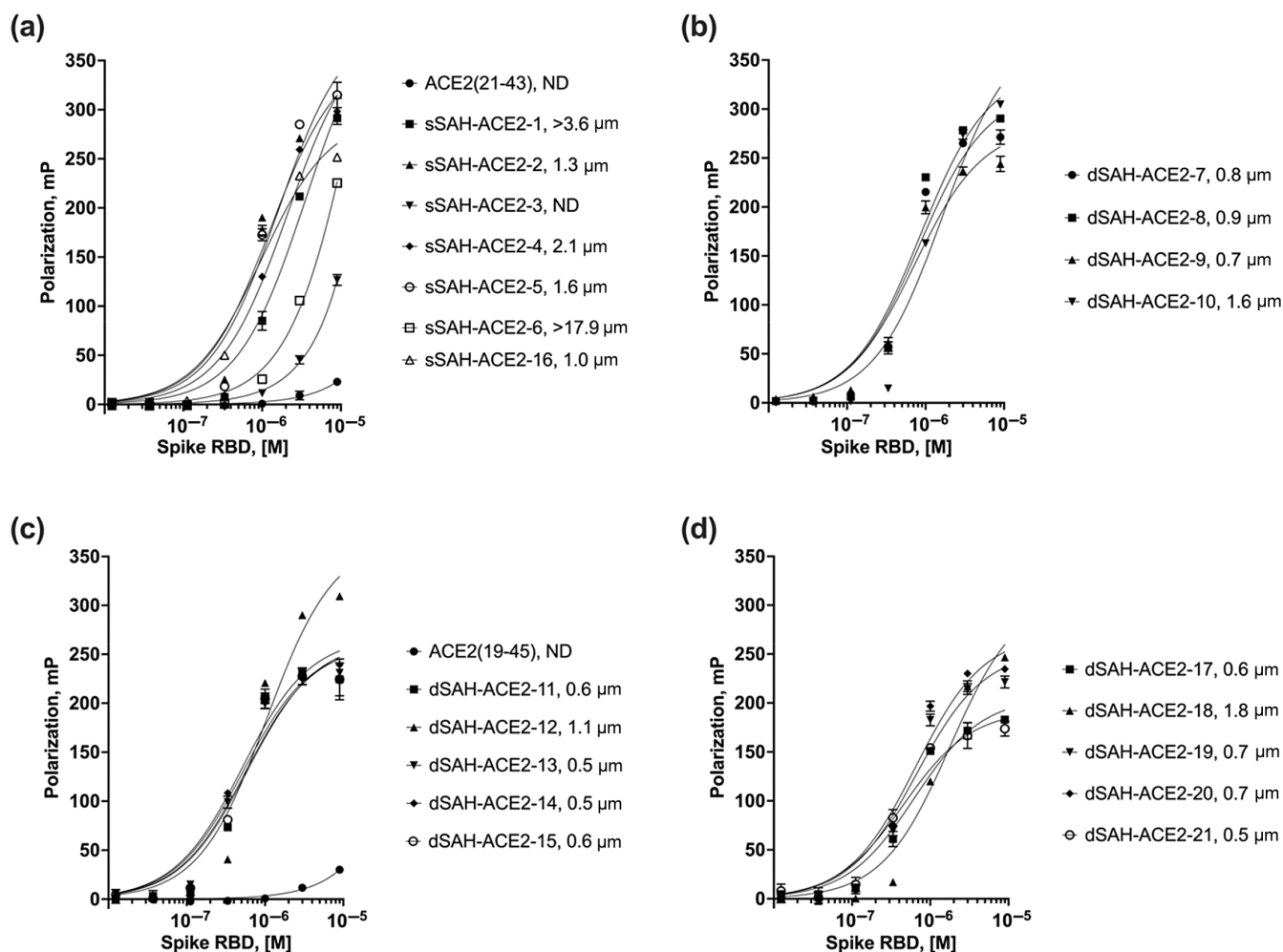
FIGURE 3 | Binding affinities of SAH ACE2 peptides to recombinant SARS-CoV-2 spike RBD protein as measured by fluorescent polarization. Binding of sSAHs (a) did not plateau and fitted poorly to the one-site binding model. In contrast, dSAHs (b–d) displayed more saturated binding curves with micromolar affinities. Unstapled peptides showed no measurable binding. Fitted K_d values are listed next to indicated constructs. Peptides are grouped on separate panels similar to Figure 2. K_d values for stapled peptides that did not plateau with binding to RBD target were noted to be above (>) the maximal extrapolated binding calculation.

clear saturation (Figure 3). These results indicate a significant fold increase in affinities among double-stapled peptides over single-stapled peptides. Differences in α-helicity in dSAHS were influenced by factors including peptide length, specific point mutations, and staple positions (Figure 2). Contrary to our initial hypothesis, we found no correlation between α-helicity and binding affinity among dSAHs. Despite significant differences in α-helicity among dSAH-ACEs (from 31.1% to 75.6% at 35°C), these ranges did not correspond with variations in binding affinity, with K_d values ranging from 500 nM to 1.6 μM (Figure 3b–d). These results suggest that there are other factors, beyond strict conservancy of α-helicity, which influence binding between stapled ACE2 peptides and the RBD target protein.

3.4 | Ability of SAH ACE2 Peptides to Block SARS-CoV-2 Infection

The biological efficacies of all 23 peptides (Table 1) were next evaluated using a SARS-CoV-2 viral neutralization assay based upon previously validated work [21]. ACE2 expressing human

lung epithelial lung carcinoma cells (A549 cells) are simultaneously infected with SARS-CoV-2 virus along with increasing doses of SAH ACE2 peptides (Figure 4a). Surviving cells were measured 3 days following infection and treatment. Peptides that protected cells from viral-induced cell death included unstapled peptides ACE2(21–43) and ACE2(19–45), a single single-stapled SAH (sSAH-ACE2-1), and multiple double-stapled SAHs (dSAH-ACE2 10, 11, 15, 17, 19, 20, 21) (Figures 4b,c and S6). Notably, related peptides dSAH-ACE2-19, 20, and 21 showed the most robust ability to prevent SARS-CoV-2-mediated cell death (Figure 4c). We found great variation in the levels of α-helical secondary structures among the inhibiting SAHs (Figure 2). This included cell death inhibition by the unstapled peptide controls, which showed little to no α-helicity or measured target binding (Figures 2 and 3).

4 | Discussion

When evaluated separately, individual assays used in this and other reports regarding the use of hydrocarbon-stapled peptides
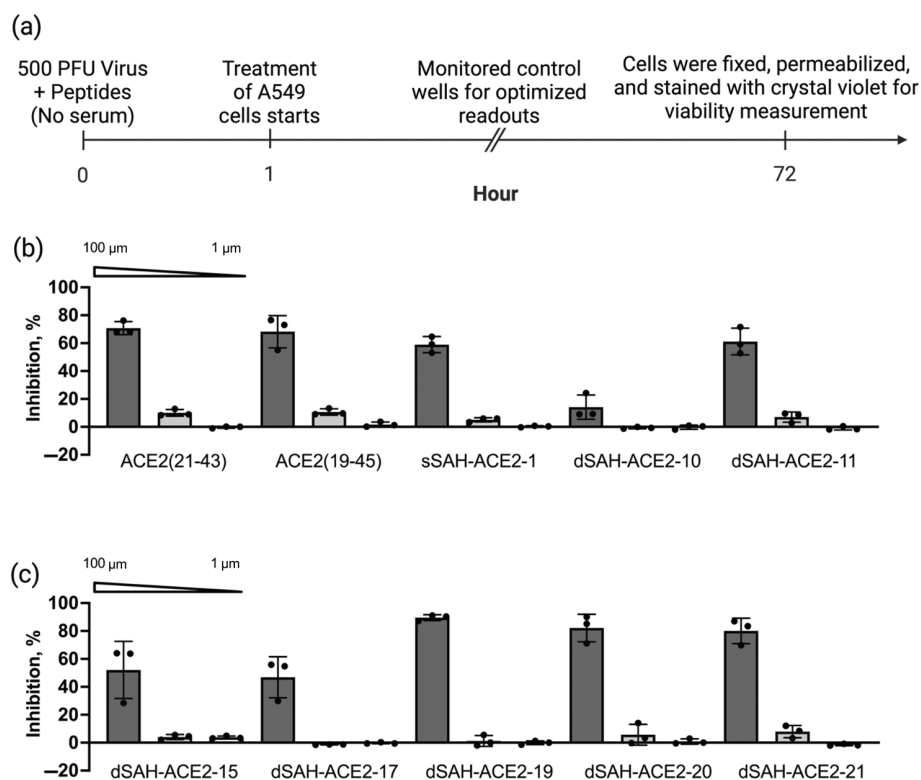
FIGURE 4 | Viral inhibition assay with live SARS-CoV-2. (a) Treatment schedule and cell death analysis of human ACE2-A549 cells infected with SARS-CoV-2 and treated with SAH-ACE2 peptides. (b,c) Percent inhibition of ACE2-A549 cell death following peptide treatment compared with untreated SARS-CoV-2-infected cells. SAHs not shown in this figure showed no cell death inhibition and are reported in Figure S6. Percent inhibition per peptide is shown in the order of 100, 10, and 1 μM.

to block the SARS-CoV2 Spike-protein:ACE2 PPI tells its own story, indicating a unique yet limited perspective of stapled peptide design. However, when viewed collectively, we believe that these experiments offer intriguing insights into this specific PPI and have implications that extend to stapled peptide design in general.

4.1 | Structural Fidelity Is the Most Important Design Parameter for Stapled Peptides Aimed at Disrupting the ACE2:SARS-CoV-2 Spike PPI

One of the key insights from this study is that both entropy and enthalpy play crucial roles in determining the binding affinity and activity of stapled peptides [30]. Ideally, a stapled peptide designed for the purpose of disruption of ACE2:Spike RBD PPI should adopt a conformation that closely resembles key structural features of the α1 helix depicted in Figure 1b. However, the use of hydrocarbon i, $i+4$ staples appeared to impose limitations by favoring rigid α-helical structures along the z-axis, thereby lacking the ability to mimic the H34 bend observed in the native structure. This mismatch between the stapled peptides and the native conformation could explain why double-stapled peptides with helicities exceeding 75% were able to effectively block virus-induced cell death only at micromolar concentrations in vitro. Similar trends can be expected with i, $i+7$ stapling, as adopted by Curreli, et al. [8] Here, peptides with more extensive stapling resulted in higher α-helical propensity (up to 80%), however, the antiviral

activity measured using a multicycle infection assay with replication-competent authentic SARS-CoV-2 resulted in IC_{100} of 17.2 μM at the lowest. Much like what we observed, such efficacy is promising, but lower than expected considering the high α-helical propensity that these peptides displayed. This is most likely due to the lack of conformation recapitulation from a straight α-helix.

Interestingly, our data also point to a cooperative effect on helix induction as influenced by the overall distance between staples. While a staple in the middle of a peptide would propagate helicity bidirectionally, as demonstrated in Figure 2c,d, when the staples were placed further apart from one another, the fold increase in helicity induced following the addition of the second staple is significantly less compared with when the two staples are closer together. This may suggest that the cooperative effect in overall helix formation for peptides with multiple staples diminishes as the distance between staples increases.

4.2 | Stapled Peptide Chain Flexibility Appears Beneficial for Therapeutic ACE2:SARS-CoV-2 Spike PPI Disruption

Extensive stapling has been recognized as beneficial for stabilizing the α-helicities of long amino acid sequences, such as those within the ACE2 α1 helix necessary to bind the spike protein RBD domain, to guarantee α-helical content and reduce

proteolysis [31, 32]. Solid-phase synthesized α-helical peptides are inherently more flexible in their unbound state. Therefore, unlike naturally occurring α-helices that exist within the greater tertiary structure of their nascent proteins, a large entropy "penalty" is incurred when these peptides bind their target. Hydrocarbon stapling serves to mitigate this entropic penalty by imposing structural constraints on the peptides alone. It is natural to assume that adding additional hydrocarbon staples would further enhance this reduction in entropic penalty, leading to peptides with more favorable binding thermodynamics. The expectation is that the additional staples would result in binders with improved energetics, making them more favorable in terms of their affinity, and possibly, their selectivity for target protein interactions.

The constraint imposed by multiple $i, i+4$ staples may have led to unfavorable enthalpic changes in the SAH-ACE2 peptide-S protein complexation process due to the native bend around the H34 position. This highly α-helical conformation proved to be structurally incompatible. Conversely, we believe that ACE2 peptides having less or no stapling at all possessed just enough chain flexibility to compensate for the overall entropic penalty, as shown by the mild yet significant levels of inhibition in vitro by unstapled controls ACE2(21–43) and ACE2(19–45). Recognizing the importance of structural fidelity and mid-chain flexibility, we synthesized sSAH-ACE2-16 and dSAH-ACE2-17 through 21, which exhibited decreased α-helical content but greater flexibility near the H34 bend by having both staples far from the bent location. These peptides emerged as the most effective viral cell death inhibitors in our library. We believe that this finding indicates a promising direction for the use of hydrocarbon $i, i+4$ staples in similar ACE2 constructs moving forward. While separation of the hydrocarbon staples is key for flexibility, we have not tested a series of double-stapled peptides with staples installed progressively further apart on a consistent primary sequence, between which we could fully interrogate the relationship between interstaple distance and secondary structure of this α-helix. Alternatively, exploring different stapling chemistry, such as an $i, i+3$ staple [33] as opposed to $i, i+7$ staples, across the H34 position, could potentially induce the desired helix bending and result in more promising anti-SARS-CoV-2 candidates.

Discordance between structure and function with respect to hydrocarbon-stapled peptides has been reported in a number of other non-helix-in-groove PPIs. In fact, we recently reported the biologic effectiveness of a hydrocarbon-stapled peptide mimetic aimed at disrupting a coiled-coil PPI [18]. Here, while double-stapled SAHs conferred biophysical advantages such as helix stability and proteolytic resistance compared with single-stapled peptides, we found that a more flexible and less α-helical SAH resulted in the best biologic effect. Similar discordance between helicity and biologic efficacy has also been measured in stapled peptides designed to disrupt other non-helix-in-groove PPIs such as those made to inhibit the fusogenic 6-helix bundle that enables respiratory syncytial virus (RSV) to penetrate target cell membranes and in HIV-1-stapled peptides designed to engage neutralizing antibodies [31, 34]. These results and those in this report highlight the continued importance of multimodal and orthogonal testing of stapled peptides designed to disrupt non-helix-in-groove PPIs.

5 | Conclusion

This study represents the synthesis of the most extensive stapled ACE2 peptide library to date, incorporating diverse design and sequence strategies. Through biophysical and biological assessments, this study provides insights that challenge the conventional emphasis on achieving high α-helicity content. Our findings highlight the importance of incorporating mid-chain flexibility for optimal results against this PPI. Moreover, we propose the exploration of alternative stapling chemistry which may provide improved bond angle recapitulation compared with $i, i+4$ staples. We believe that these insights contribute to advancing the design and optimization of stapled ACE2 peptides and those for other similar applications.

Conflicts of Interest

The authors declare no conflicts of interest.

Data Availability Statement

All data generated and analyzed during this study is available from the corresponding author upon reasonable request.

References

1. I. F. Miller, A. D. Becker, B. T. Grenfell, and C. J. E. Metcalf, "Disease and Healthcare Burden of COVID-19 in the United States," *Nature Medicine* 26 (2020): 1212–1217.

2. T. Asselah, D. Durantel, E. Pasmant, G. Lau, and R. F. Schinazi, "COVID-19: Discovery, Diagnostics and Drug Development," *Journal of Hepatology* 74 (2021): 168–184.

3. M. Hoffmann, H. Kleine-Weber, S. Schroeder, et al., "SARS-CoV-2 Cell Entry Depends on ACE2 and TMPRSS2 and Is Blocked by a Clinically Proven Protease Inhibitor," *Cell* 181 (2020): 271–280.e8.

4. R. Yan, Y. Zhang, Y. Li, L. Xia, Y. Guo, and Q. Zhou, "Structural Basis for the Recognition of SARS-CoV-2 by Full-Length Human ACE2," *Science* 367 (2020): 1444–1448.

5. D. J. Benton, A. G. Wrobel, P. Xu, et al., "Receptor Binding and Priming of the Spike Protein of SARS-CoV-2 for Membrane Fusion," *Nature* 588 (2020): 327–330.

6. L. J. de Campos, N. Y. Palermo, and M. Conda-Sheridan, "Targeting SARS-CoV-2 Receptor Binding Domain With Stapled Peptides: AnIn SilicoStudy," *Journal of Physical Chemistry. B* 125 (2021): 6572–6586.

7. D. C. Morgan, C. Morris, A. Mahindra, et al., "StapledACE2peptidomimetics Designed to Target theSARS-CoV-2 Spike Protein Do Not Prevent Virus Internalization," *Peptide Science (Hoboken, N.J.)* 113 (2021): e24217.

8. F. Curreli, S. M. B. Victor, S. Ahmed, et al., "Stapled Peptides Based on Human Angiotensin-Converting Enzyme 2 (ACE2) Potently Inhibit SARS-CoV-2 InfectionIn Vitro," *MBio* 11 (2020): e02451-20.

9. L. Calugi, G. Sautariello, E. Lenci, et al., "Identification of a Short ACE2-Derived Stapled Peptide Targeting the SARS-CoV-2 Spike Protein," *European Journal of Medicinal Chemistry* 249 (2023): 115118.

10. M. N. Maas, J. C. J. Hintzen, P. M. G. Löffler, and J. Mecinović, "Targeting SARS-CoV-2 Spike Protein by Stapled hACE2 Peptides," *Chemical Communications (Cambridge, England)* 57 (2021): 3283–3286.

11. S. Tzotzos, "Stapled Peptides as Potential Inhibitors of SARS-CoV-2 Binding to the hACE2 Receptor," *Journal of Peptide Science* 28 (2022): e3409.

12. G. H. Bird, E. Mazzola, K. Opoku-Nsiah, et al., "Biophysical Determinants for Cellular Uptake of Hydrocarbon-Stapled Peptide Helices," *Nature Chemical Biology* 12 (2016): 845–852.

13. G. H. Bird, W. C. Crannell, and L. D. Walensky, "Chemical Synthesis of Hydrocarbon-Stapled Peptides for Protein Interaction Research and Therapeutic Targeting," *Current Protocols in Chemical Biology* 3 (2011): 99–117.

14. A. Hadji, G. K. Schmitt, M. R. Schnorenberg, et al., "Preferential Targeting of MCL-1 by a Hydrocarbon-Stapled BIM BH3 Peptide," *Oncotarget* 10 (2019): 6219–6233.

15. J. L. Labelle, S. G. Katz, G. H. Bird, et al., "A Stapled BIM Peptide Overcomes Apoptotic Resistance in Hematologic Cancers," *Journal of Clinical Investigation* 2012 (2018): 122–2031.

16. M. R. Schnorenberg, J. A. Bellairs, R. Samaeekia, H. Acar, M. V. Tirrell, and J. L. Labelle, "Activating the Intrinsic Pathway of Apoptosis Using BIM BH3 Peptides Delivered by Peptide Amphiphiles With Endosomal Release," *Materials* 12 (2019): 2567.

17. G. H. Bird, N. Madani, A. F. Perry, et al., "Hydrocarbon Double-Stapling Remedies the Proteolytic Instability of a Lengthy Peptide Therapeutic," *Proceedings of the National Academy of Sciences of the United States of America* 107 (2010): 14093–14098.

18. K. M. Hawley, R. J. Eclov, M. R. Schnorenberg, et al., "Inhibition of FOXP3 by Stapled Alpha-Helical Peptides Dampens Regulatory T Cell Function," *Proceedings of the National Academy of Sciences of the United States of America* 119 (2022): e2209044119.

19. A. Chakrabartty, T. Kortemme, S. Padmanabhan, and R. L. Baldwin, "Aromatic Side-Chain Contribution to Far-Ultraviolet Circular Dichroism of Helical Peptides and Its Effect on Measurement of Helix Propensities," *Biochemistry* 32 (1993): 5560–5565.

20. J. M. Scholtz, H. Qian, E. J. York, J. M. Stewart, and R. L. Baldwin, "Parameters of Helix–Coil Transition Theory for Alanine-Based Peptides of Varying Chain Lengths in Water," *Biopolymers* 31 (1991): 1463–1470.

21. L. R. Volpatti, R. P. Wallace, S. Cao, et al., "Polymersomes Decorated With the SARS-CoV-2 Spike Protein Receptor-Binding Domain Elicit Robust Humoral and Cellular Immunity," *ACS Central Science* 7 (2021): 1368–1380.

22. D. Blanco-Melo, B. E. Nilsson-Payant, W. C. Liu, et al., "Imbalanced Host Response to SARS-CoV-2 Drives Development of COVID-19," *Cell* 181 (2020): 1036–1045.e9.

23. Y. S. Tan, D. P. Lane, and C. S. Verma, "Stapled Peptide Design: Principles and Roles of Computation," *Drug Discovery Today* 21 (2016): 1642–1653.

24. T. Sitthiyotha and S. Chunsrivirot, "Computational Design of 25-Mer Peptide Binders of SARS-CoV-2," *Journal of Physical Chemistry B* 124 (2020): 10930–10942.

25. K. K. Chan, D. Dorosky, P. Sharma, et al., "Engineering Human ACE2 to Optimize Binding to the Spike Protein of SARS Coronavirus 2," *Science* 369 (2020): 1261–1265.

26. C. E. Schafmeister, J. Po, and G. L. Verdine, "An All-Hydrocarbon Cross-Linking System for Enhancing the Helicity and Metabolic Stability of Peptides," *Journal of the American Chemical Society* 122 (2000): 5891–5892.

27. P. S. Kutchukian, J. S. Yang, G. L. Verdine, and E. I. Shakhnovich, "All-Atom Model for Stabilization of α-Helical Structure in Peptides by Hydrocarbon Staples," *Journal of the American Chemical Society* 131 (2009): 4622–4627.

28. A. Maity, A. R. Choudhury, and R. Chakrabarti, "Effect of Stapling on the Thermodynamics of mdm2–p53 Binding," *Journal of Chemical Information and Modeling* 61 (2021): 1989–2000.

29. G. H. Bird, F. Bernal, K. Pitter, and L. D. Walensky, "Chapter 22 Synthesis and Biophysical Characterization of Stabilized α-Helices of BCL-2 Domains," *Methods in Enzymology* 446 (2008): 369.

30. A. R. Choudhury, A. Maity, S. Chakraborty, and R. Chakrabarti, "Computational Design of Stapled Peptide Inhibitor Against SARS-CoV-2 Receptor Binding Domain," *Peptide Science (Hoboken, N.J.)* 114 (2022): e24267.

31. G. H. Bird, S. Boyapalle, T. Wong, et al., "Mucosal Delivery of a Double-Stapled RSV Peptide Prevents Nasopulmonary Infection," *Journal of Clinical Investigation* 124 (2014): 2113–2124.

32. G. H. Bird, A. Fu, S. Escudero, et al., "Hydrocarbon-Stitched Peptide Agonists of Glucagon-Like Peptide-1 Receptor," *ACS Chemical Biology* 15 (2020): 1340–1348.

33. S. Y. Shim, Y. W. Kim, and G. L. Verdine, "A Newi, i + 3 Peptide Stapling System for α-Helix Stabilization," *Chemical Biology & Drug Design* 82 (2013): 635–642.

34. G. H. Bird, A. Irimia, G. Ofek, P. D. Kwong, I. A. Wilson, and L. D. Walensky, "Stapled HIV-1 Peptides Recapitulate Antigenic Structures and Engage Broadly Neutralizing Antibodies," *Nature Structural & Molecular Biology* 21 (2014): 1058–1067.

Supporting Information

Additional supporting information can be found online in the Supporting Information section.